AGU PUBLICATIONS

Geophysical Research Letters

RESEARCH LETTER
10.1002/2016GL068313

Key Points:
- Based on two special chorus events, we propose a new potential generation mechanism for multiband chorus
- Lower band cascade involves the wave-wave coupling between lower band chorus and the density mode
- Amplitude threshold of lower band cascade is anticorrelated with wave normal angle and frequency

Correspondence to:
Q. Lu,
qmlu@ustc.edu.cn

Citation:
Gao, X., Q. Lu, J. Bortnik, W. Li, L. Chen, and S. Wang (2016), Generation of multiband chorus by lower band cascade in the Earth's magnetosphere, *Geophys. Res. Lett.*, *43*, 2343–2350, doi:10.1002/2016GL068313.

Received 17 FEB 2016
Accepted 1 MAR 2016
Accepted article online 6 MAR 2016
Published online 16 MAR 2016

Generation of multiband chorus by lower band cascade in the Earth's magnetosphere

Xinliang Gao[1,2], Quanming Lu[1,2], Jacob Bortnik[3], Wen Li[3], Lunjin Chen[4], and Shui Wang[1,2]

[1]CAS Key Laboratory of Geospace Environment, Department of Geophysics and Planetary Science, University of Science and Technology of China, Hefei, China, [2]Collaborative Innovation Center of Astronautical Science and Technology, Hefei, China, [3]Department of Atmospheric and Oceanic Sciences, University of California, Los Angeles, California, USA, [4]Department of Physics, University of Texas at Dallas, Richardson, Texas, USA

Abstract Chorus waves are intense electromagnetic whistler mode emissions in the magnetosphere, typically falling into two distinct frequency bands: a lower band (0.1–0.5f_{ce}) and an upper band (0.5–0.8f_{ce}) with a power gap at about 0.5f_{ce}. In this letter, with the Time History of Events and Macroscale Interactions during Substorms satellite, we observed two special chorus events, which are called as multiband chorus because upper band chorus is located at harmonics of lower band chorus. We propose a new potential generation mechanism for multiband chorus, which is called as lower band cascade. In this scenario, a density mode with a frequency equal to that of lower band chorus is generated by the ponderomotive effect (inhomogeneity of the electric amplitude) along the wave vector, and then upper band chorus with the frequency twice that of lower band chorus is generated through wave-wave couplings between lower band chorus and the density mode. The mechanism provides a new insight into the evolution of whistler mode chorus in the Earth's magnetosphere.

1. Introduction

Chorus waves are intense electromagnetic whistler mode emissions detected ubiquitously in the Earth's inner magnetosphere, getting their name from the audible sound after converted by a radio receiver [*Bianchi and Meloni*, 2007], which resembles a chorus of chirping birds. The local acceleration by chorus waves is considered to be the main source of relativistic electrons in the Van Allen radiation belt [*Reeves et al*., 2013; *Thorne et al*., 2013], which pose a threat to satellites and humans in space. Furthermore, chorus waves are also the dominant cause of the strong diffuse auroral precipitation into the Earth's atmosphere [*Thorne et al*., 2010; *Nishimura et al*., 2013], leading to enhanced ionization and chemical changes of the atmosphere. The earliest satellite observations of chorus waves can trace back to the late 1960s [*Burtis and Helliwell*, 1969], when this new type of VLF (very low frequency) radiation was at first recorded by OGO 1 and OGO 3 in the Earth's magnetosphere. During the following decades, a large amount of observed data has been collected by various satellites (Cluster, Time History of Events and Macroscale Interactions during Substorms (THEMIS), Van Allen Probes, etc), which provides a more comprehensive picture of chorus waves. Chorus waves are preferentially detected in the low-density region outside the plasmapause [*LeDocq et al*., 1998], which appear as either rising tones, falling tones, or hiss-like emissions in the frequency-time spectrogram [*Li et al*., 2012; *Gao et al*., 2014]. In addition, they usually occur in two distinct frequency bands [*Tsurutani and Smith*, 1974]: a lower band (0.1–0.5f_{ce} and f_{ce} is the equatorial electron gyrofrequency) and an upper band (0.5–0.8f_{ce}) with a remarkable power minimum at about 0.5f_{ce}. There have been numerous mechanisms proposed to explain the generation of upper band chorus, which can be roughly divided into two main categories: (1) upper band chorus is just the extension of lower band chorus, but with a strong nonlinear damping at about 0.5f_{ce} [*Omura et al*., 2009], and (2) lower and upper band waves are generated in different source regions [*Bell et al*., 2009] or by different electron populations [*Fu et al*., 2014]. However, both candidates lack direct observational evidences. Here by analyzing two special chorus events observed by the THEMIS satellite, where upper band chorus is located at harmonics of lower band chorus, we propose a new mechanism, named as lower band cascade, to explain the generation of such kind of upper band chorus.

2. THEMIS Data Analysis

The THEMIS spacecraft [*Angelopoulos*, 2008], including five identical probes (THEMIS A, B, C, D, and E), are orbiting in the near-equatorial magnetosphere, where chorus waves are typically detected. The THEMIS

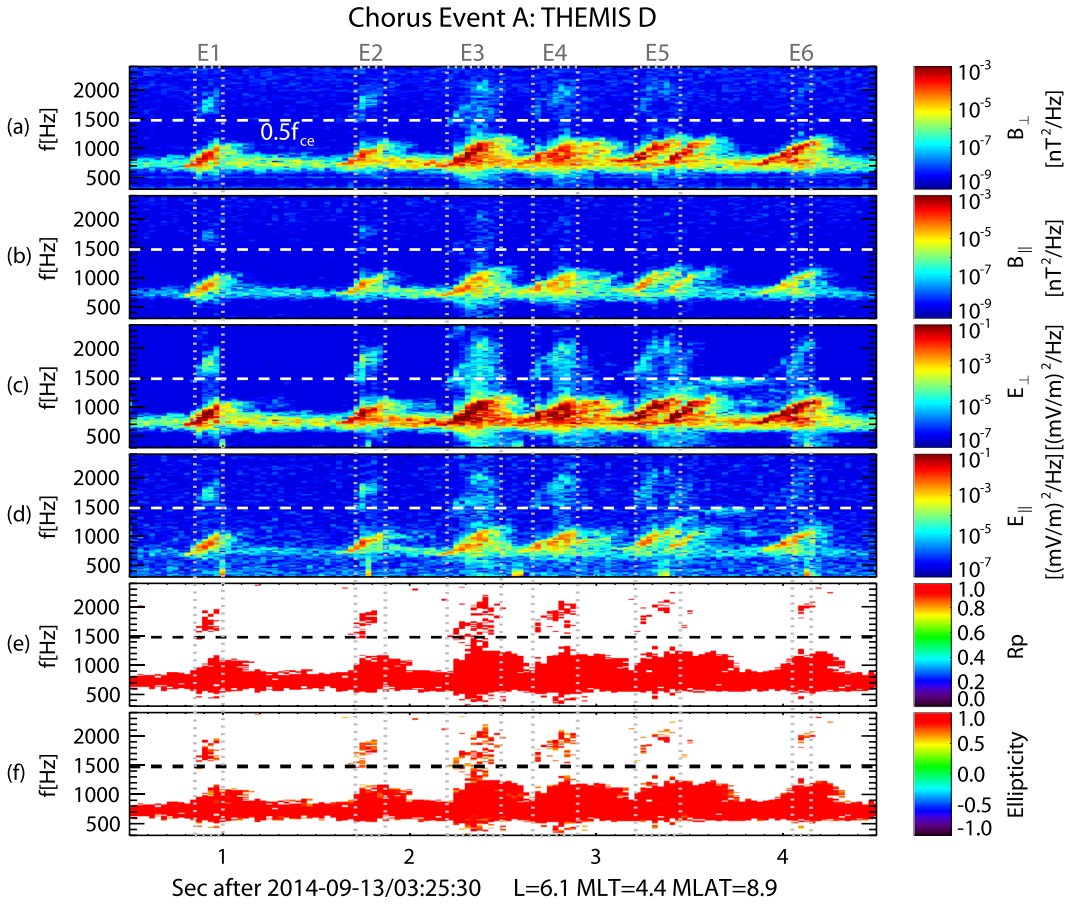

Figure 1. Time evolution of (a–d) the spectrogram of perpendicular and parallel electromagnetic fields ($B_{\perp}$, $B_{||}$, $E_{\perp}$, and $E_{||}$), (e) the polarization ratio R_p, and (f) the ellipticity. In all panels, the dashed horizontal lines in white or black represent $0.5f_{ce}$. All six elements of upper band chorus are marked by gray vertical dotted lines and then named as E1–E6 following the time sequence.

spacecraft can provide waveform data with a sampling frequency of up to ~16 kHz, which are recorded simultaneously from Search-Coil Magnetometer [*Roux et al.*, 2008] and Electric Field Instrument [*Bonnell et al.*, 2008]. Here the waveform data have been rotated into the field-aligned coordinate system with the z axis aligned with the ambient magnetic field. The polarization information (such as polarization ratio R_p, ellipticity, and wave normal angle θ_k) of chorus waves is extracted from magnetic wave burst data through the method introduced by *Bortnik et al.* [2007]. Note that the obtained wave normal angles have an inherent 180° ambiguity here due to only magnetic fields involved in this procedure; therefore, all wave normal angles have been converted into values less than 90°. The background magnetic fields are measured by the Fluxgate Magnetometer [*Auster et al.*, 2008], and the equatorial electron gyrofrequency f_{ce} is calculated on the assumption that the Earth's magnetosphere is a simple dipole field.

3. Observational Results

Figures 1a–1d illustrate the dynamic spectrogram of a chorus event (Chorus Event A), which was detected by THEMIS D on 13 September 2014 at $L = 6.1$ in the dawn sector (magnetic local time (MLT) = 4.4). This event was located just outside the typical source region of chorus waves, being located well away from the equator (~8.9°). Figure 1e shows the polarization ratio R_p, i.e., the ratio between polarized and total power, which is just used to check other calculated polarization parameters (such as wave normal angle and ellipticity) [*Bortnik et al.*, 2007], while Figure 1f shows the ellipticity. For the sake of convenience, all elements of upper band chorus are marked by gray vertical dotted lines and then named as E1–E6 following the time sequence.

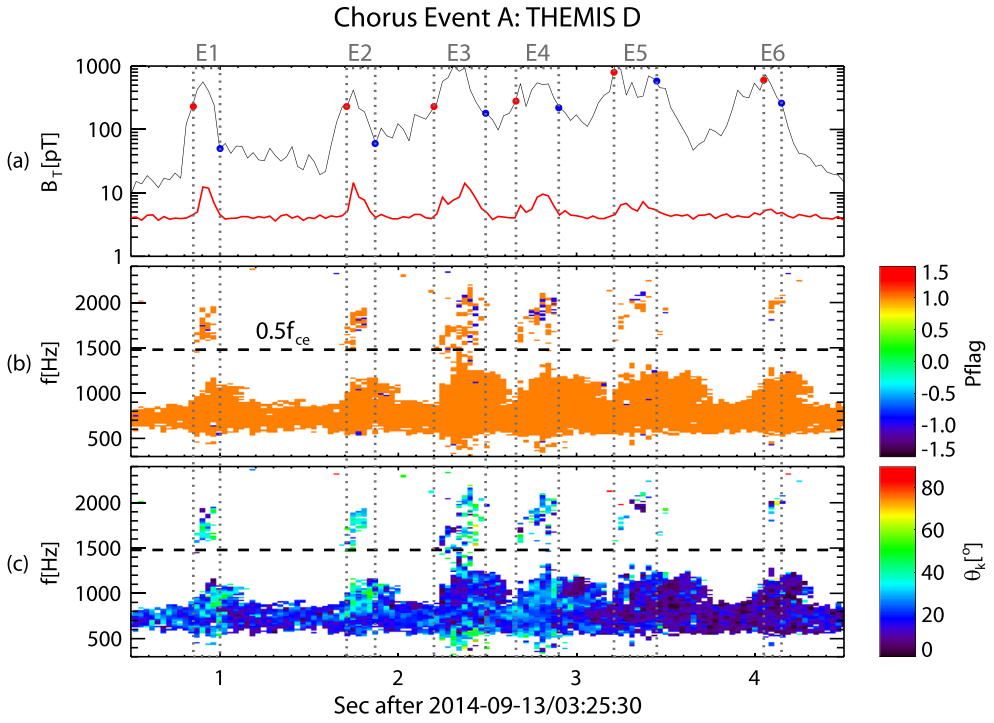

Figure 2. Time evolution of (a) magnetic amplitudes of lower (0.1–0.5f_{ce}; black line) and upper (0.5–0.8f_{ce}; red line) band chorus waves, (b) a flag, i.e., "Pflag," showing the wave propagating direction (1 for away from equator, while −1 for toward equator), and (c) the wave normal angle θ_k. The black dashed horizontal lines in Figures 2b and 2c represent 0.5f_{ce}. The starts and ends of upper band chorus elements are marked with red and blue dots, respectively.

Both lower and upper band chorus waves can be clearly observed at almost the same time, which appear as rising tones in Figures 1a–1d. As expected, they are all right-hand polarized with the large ellipticity (~1; Figure 1f). Meanwhile, the magnetic amplitude of lower band chorus is nearly 2 orders larger than that of upper band chorus. Most notably, the upper band chorus is observed nearly at the second harmonic of lower band chorus, and there is a clear power gap around 0.5f_{ce} between them.

More details about Chorus Event A are illustrated in Figure 2, which includes (a) magnetic amplitudes of lower (0.1–0.5f_{ce}; black line) and upper (0.5–0.8f_{ce}; red line) band chorus waves, (b) the wave propagating direction (1 for away from equator, while −1 for toward equator), and (c) the wave normal angle θ_k. The wave propagating direction is determined by both directions of Poynting vector and the radial component of background magnetic fields followed the method by *Li et al.* [2013]. The starts and ends of upper band chorus elements are marked with red and blue dots, respectively. Here we highlight a few features of the observed waves for further comparison between lower band chorus and upper band chorus. First, as shown in Figures 2b and 2c, both lower band chorus and upper band chorus have almost the same propagation direction and wave normal angle, which implies that the generation of upper band waves should be a one-dimensional physical process along the propagation direction (as opposed to being generated by different resonance modes). Second, the upper band chorus can be detected only when the magnetic amplitude of lower band waves reaches a certain threshold ~100 pT (Figure 2a). This could mean that some nonlinear process takes place during the excitation of the upper band waves. Furthermore, we also find that the amplitude threshold of this nonlinear process is closely dependent on the frequency and wave normal angle of lower band waves. As shown in Figure 2a, for each element, the magnetic amplitude of lower band chorus at its start (red dot; lower frequency) is much larger than that at its end (blue dot; higher frequency). Taking E1 as an example, the amplitude threshold for lower band waves at the start (~0.25f_{ce}) is about 200 pT, while the amplitude threshold for lower band waves at the end (~0.35f_{ce}) is much smaller, only about 50 pT. Comparing E1 and E5 (or E2 and E6), E5 (or E6) is more field aligned with the smaller wave normal angle, but its amplitude threshold is larger than that for E1 (or E2), and its wave amplitude of upper band waves is much smaller.

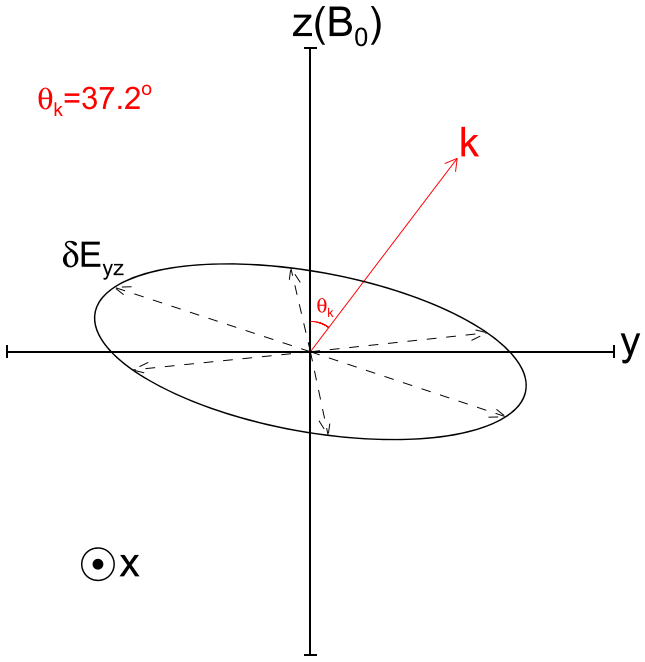

Figure 3. A schematic diagram for the wave vector and wave electric field. Here the coordinate system is same as that used above, i.e., the field-aligned coordinate system. The black ellipse describes the hodograms of wave electric fields δE_{yz} in the *yoz* plane, while the red arrow denotes the direction of the wave vector *k*.

Based on these properties, we propose a new generation mechanism for the upper band chorus, which is called as "lower band cascade." The upper band chorus (with frequencies f_h) is excited through a coupling process between lower band chorus (with frequencies f_l) and density modes (with frequencies f_n) along the propagating direction of the lower band waves. And the three wave modes should satisfy the resonant condition, i.e., $f_h = f_l + f_n$. Here the density modes can be excited due to the ponderomotive effect (inhomogeneity of the electric amplitude) of lower band waves, i.e., the fluctuating electric fields along the wave vector. This can be supported by the previous theoretical work [*Verkhoglyadova et al.*, 2010], which pointed out that the electric field polarization plane is not orthogonal to the wave vector for nonparallel propagating chorus, indicating that wave electric fields have a large component along the wave vector.

To check the angle between the wave vector and electric field, we arbitrarily pick a wave mode (~860 Hz) around the middle time of E1 and present a schematic diagram in Figure 3. Through the procedure developed by *Bortnik et al.* [2007], we can obtain the wave normal angle $\theta_k = 37.2°$, and the azimuthal angle with respect to *x* axis $\phi_k = -89.5°$, indicating *k* can be simply assumed in the *yoz* plane. In this special case, the *x* component of the wave electric field δE is always perpendicular to the wave vector, so the angle between *k* and δE is mainly determined by the wave electric field in the *yoz* plane δE_{yz}. As shown in Figure 2b, the wave vector for this chosen mode should have a positive component along the background magnetic field; therefore, *k* can be well determined in Figure 3. Through the Fourier transform of fluctuating electric fields, we can obtain not only the intensity of δE_y and δE_z for this mode but also the phase difference between them. Therefore, we can plot the hodograms of δE_{yz} in the *yoz* plane, which have been shown in Figure 3. Finally, it is clearly shown that the wave electric fields will have a large component along the wave vector, because the angle between them is not necessarily 90°. The fluctuating electric fields along the wave vector can easily cause the density modes with $f_n \approx f_l$, which then couple with lower band waves to generate upper band waves at about $2f_l$. For more oblique lower band chorus, the fluctuating electric field along the wave vector is stronger, which then results in the stronger density fluctuations, and ultimately stronger nonlinear wave-wave coupling. Besides, the growth rate of this nonlinear physical process is positively correlated with the frequency of lower band waves [*Stenflo et al.*, 1986]. These properties are quite consistent with observations shown in Figure 2.

The bicoherence index is useful to measure the amount of phase coupling that occurs among three wave modes, which is close to 1 when these signals satisfy the resonance condition [*van Milligen et al.*, 1995]. The waveform data of one perpendicular component of the magnetic field (B_x) and the parallel electric field (E_z) for a 70 ms interval around the middle time of E1 are chosen to calculate the bicoherence index. The bicoherence index is given by $\left|\left\langle E_z(f_1)B_x(f_2)B_x^*(f_3)\right\rangle\right|^2 / \left\langle\left|E_z(f_1)B_x(f_2)\right|^2\right\rangle\left\langle\left|B_x^*(f_3)\right|^2\right\rangle$ (where $f_3 = f_1 + f_2$ and the bracket $\langle\rangle$ denotes an average over the 70 ms interval) [*van Milligen et al.*, 1995], after E_z and B_x have been decomposed with the wavelet method. Figures 4a and 4b display the power spectra of E_z and B_x obtained from fast Fourier transform (FFT) transformation, while Figure 4c shows the bicoherence index between E_z

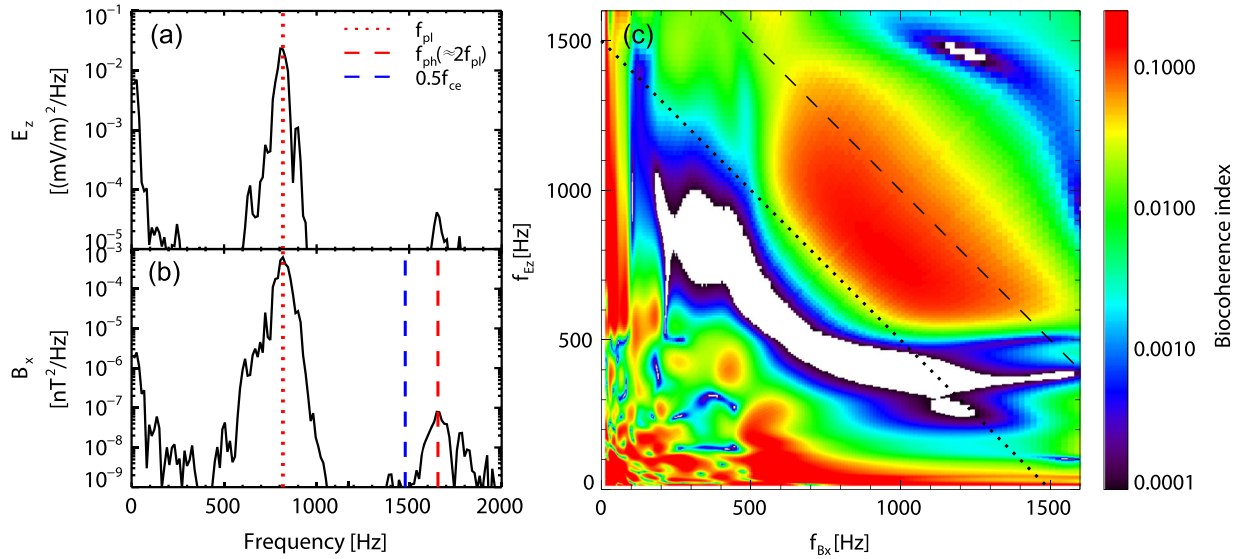

Figure 4. The power spectra obtained from FFT transformation of (a) E_z and (b) B_x, and (c) the distribution of bicoherence index in f_{Ez}-f_{Bx} domain. In Figures 4a and 4b, the red dotted and dashed vertical lines denote the peak frequencies (f_{pl} and f_{ph}) with the maximum power for lower band chorus and upper band chorus, respectively. Meanwhile, the frequency $0.5f_{ce}$ is denoted by a blue dashed vertical line. In Figure 4c, the black dotted and dashed lines correspond to $f_{Ez} + f_{Bx} = 1500$ and 2000 Hz, respectively.

and B_x. Here E_z approximately represents the density fluctuations, because the fluctuating electric fields along the wave vector have a significant contribution to E_z. In Figures 4a and 4b, the dominant power spectrum of E_z is located from about 600 to 1000 Hz, with the peak frequency $f_{pl} \approx 820$ Hz, so is B_x for lower band chorus. For upper band chorus, the dominant power spectrum of B_x is located from about 1500 to 2000 Hz, with the peak frequency $f_{ph} \approx 2f_{pl}$. In Figure 4c, the lower band chorus, density mode, and upper band chorus are denoted by f_{Bx}, f_{Ez}, and $f_{Bx} + f_{Ez}$, respectively. In other words, each bicoherence index in Figure 4c evaluates the phase coupling between the lower band chorus f_{Bx}, density mode f_{Ez}, and upper band chorus $f_{Bx} + f_{Ez}$. We find that the region with the largest bicoherence index (>0.2) is mainly located within the spectral range of E_z (Figure 4a) and B_x (Figure 4b) of lower band waves, which indicates their strong phase couplings during E1. Moreover, just as we expected, the observed upper band chorus ($f_{Bx} + f_{Ez}$) falls well within the region of strong couplings, whose frequency range (1500–2000 Hz) is marked between the dotted and dashed lines in Figure 4c.

In addition, another strong wave-wave coupling chorus event (Chorus Event B) is shown in Figure 5 to further support our proposed lower band cascade mechanism for the generation of upper band chorus. Figures 5 illustrates (a) magnetic amplitudes of lower (0.1–0.5f_{ce}; black line) and upper (0.5–1f_{ce}; red line) band chorus waves, (b–e) the dynamic spectra of perpendicular and parallel electric and magnetic fields in the field-aligned coordinate, (f) the wave propagating direction, and (g) the wave normal angle θ_k. All the elements are marked by gray vertical dotted lines and named as E1*–E3* following the time sequence. For clarity, the peak frequency (dominant power) of lower band chorus and its twice and triple frequencies are marked with the plus symbol in each element in Figure 5d, which is quite consistent with the spectrogram. Chorus Event B was detected by THEMIS D on 5 April 2013, at $L = 11.1$, and in the dawn sector (MLT = 6.6). Besides the properties already pointed out in Chorus Event A, what is most striking in this event is the three-band structure (lower band chorus, its second and third harmonics) of rising tones (Figures 5b–5e). Although the magnetic amplitude of lower band chorus (Figure 5a) is similar to that in Chorus Event A (Figure 2a), the background magnetic field at $L = 11.1$ should be much smaller than that at $L = 6.1$, which means that the normalized amplitude (normalized by the background magnetic field) is much larger in Chorus Event B. Based on a similar bicoherence analysis (not shown) to Figure 4, the lower band chorus f_l can not only couple with the density modes with $f_n \approx f_l$ but also couple with the density modes with $f_n \approx 2f_l$. Curiously, we note that for E1* and E2*, there is no evidence for the typical power gap around $0.5f_{ce}$, but rather at about 0.4 and $0.6f_{ce}$.

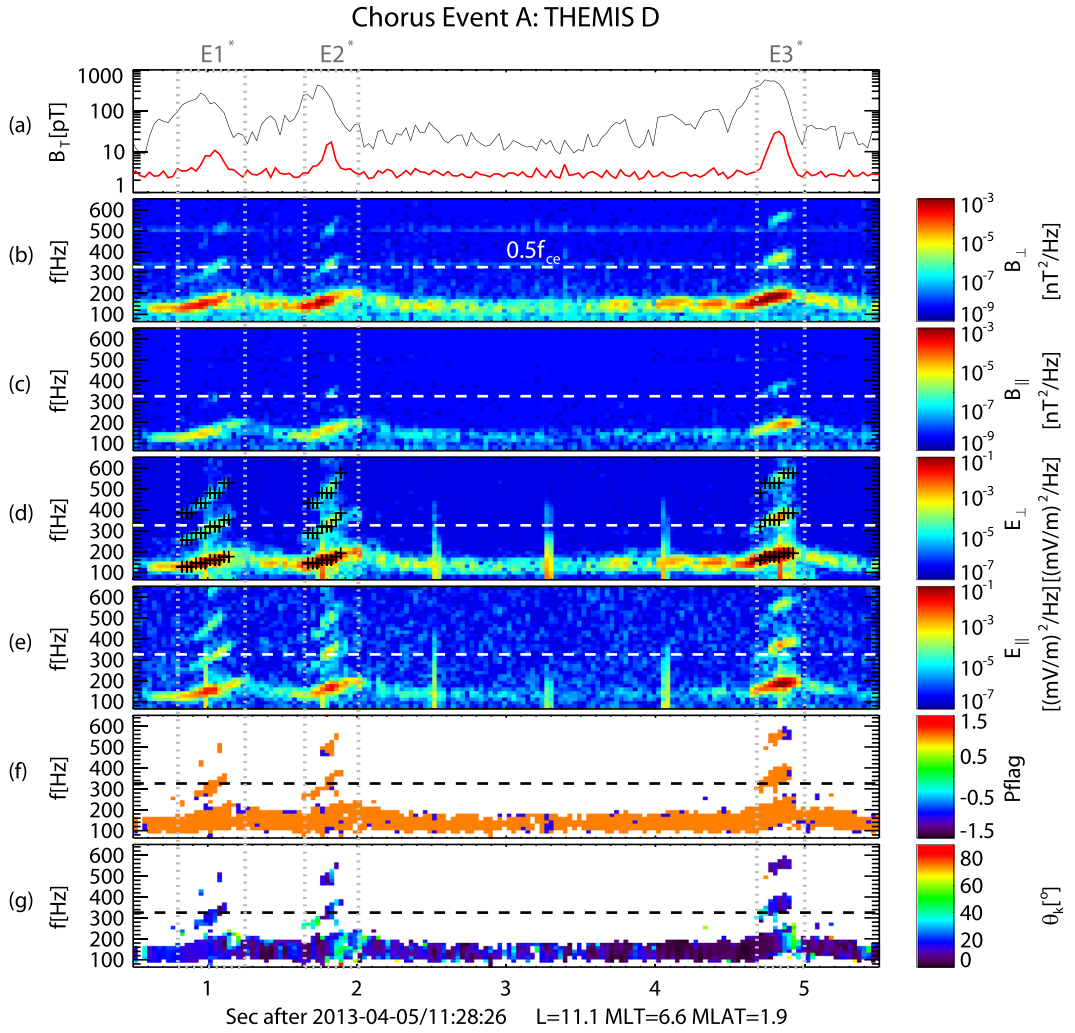

Figure 5. Time evolution of (a) magnetic amplitudes B_T of lower (0.1–0.5f_{ce}; black line) and upper (0.5–0.8f_{ce}; red line) band chorus, (b–e) the spectrogram of perpendicular and parallel electromagnetic fields ($B_{\perp}$, $B_{||}$, $E_{\perp}$, and $E_{||}$), (f) a flag, i.e., Pflag, showing the wave propagating direction, and (g) the wave normal angle θ_k. In Figures 5b–5g, the dashed horizontal lines in white or black represent 0.5f_{ce}. All three elements of upper band chorus are marked by gray vertical dotted lines and then named as E1*–E3* following the time sequence. In Figure 5b, the peak frequency (dominant power) of lower band chorus and its twice and triple frequencies are marked with the plus symbol in each element.

4. Conclusion and Discussion

In this letter, based on in situ observations of two chorus events (Chorus Events A and B) by the THEMIS D satellite, we report a special kind of chorus, which is called as multiband chorus. In multiband chorus, upper band chorus is located at harmonics of lower band chorus and has a much smaller amplitude. For the first time, we propose a new mechanism, named as lower band cascade, as a potential generation mechanism for such kind of upper band chorus. In this scenario, a density mode with a frequency equal to that of the lower band chorus is excited due to the ponderomotive effect along the wave vector, and then an upper band chorus with the frequency twice that of the lower band chorus is generated through the wave-wave coupling between the lower band chorus and the density mode. Moreover, the amplitude threshold of lower band cascade for lower band chorus waves is found to be inversely correlated with the wave normal angle and wave frequency.

The steepening of compressional waves is also a possible way to generate the harmonics [*Smerd*, 1955]. However, according to the previous study by *Yoon et al.* [2014], the steepening process is extremely difficult to occur in the magnetosphere, unless the whistler mode waves have very large wave amplitude (>5000 pT,

or $\delta B/B_0 > 0.05$ in the radiation belt) and wave normal angle close to the resonant angle. In our observations, the wave normal angle is about 30°–40°, much smaller than the resonant angle (~70°). Therefore, the steepening process can be excluded in our events, because both the wave amplitude and wave normal angle are much smaller (Figures 2 and 5) than the threshold. Meanwhile, the waveform during chorus events in this study has also been checked (not shown), and no steepening is observed. One thing we should emphasize is that the wave coupling process involves the coupling not only between the wave frequencies but also between the wave numbers. However, due to the single-satellite observation, there is a common difficulty in determining wave numbers, especially for the density mode and lower band chorus with almost the same frequency. Besides, there are a lot of uncertainties in the current plasma measurement, and the dispersion relation describing the coupling between whistler mode waves and density fluctuations is still unclear. This makes it impossible to estimate the wave numbers through the fluctuating electromagnetic fields. Then we cannot directly check the coupling between wave numbers in this study. How the coupling conditions between the wave frequencies and wave numbers are satisfied could only be investigated from a theoretical point. This is interesting but beyond the scope of this letter.

The wave-wave coupling between lower band waves and density fluctuations can generate upper band waves at about the second (Chorus Event A), and even the third (Chorus Event B) harmonics of the lower band waves. As shown in Figure 2a, the amplitude threshold of lower band cascade is just about 100 pT at $L = 6.1$, and even lower for higher frequencies, larger L shells, and larger wave normal angles. According to previous observations [*Li et al*., 2011], the lower band chorus waves with amplitudes larger than 100 pT often occur in the Earth's magnetosphere, making the amplitude threshold easily satisfied, so the lower band cascade may occur commonly. However, through the lower band cascade process, upper band chorus will be generated with an amplitude 1–2 orders of magnitude smaller than that of lower band chorus (Figures 2a and 5a), which is weaker than the typical upper band chorus exhibited in the previous work [*Santolik et al*., 2003]. Therefore, we conclude that the lower band cascade provides a potential generation mechanism for multiband chorus observed in Earth's magnetosphere. Actually, we have found that there are over 400 chorus events involving the lower band cascade detected by THEMIS satellites (THA, THD, and THE) during 2008–2015. A statistical study is still necessary to quantitatively evaluate the contribution of the lower band cascade for the generation of upper band chorus and whether such kind of mechanism can be applied to a more general situation.

Acknowledgments

This research was supported by the NSFC grants 41331067, 41474125, 11235009, and 41421063 and 973 program (2012CB825602 and 2013CBA01503), and the Fundamental Research Funds for the Central Universities. J. Bortnik would like to thank NASA grant NNX13AI61G for support of his time. L. Chen acknowledges the support of NSF grant AGS-1405041. We also acknowledge the entire THEMIS instrument group and the THEMIS data used in this letter obtained from http://themis.ssl.berkeley.edu/data/themis.

References

Angelopoulos, V. (2008), The THEMIS mission, *Space Sci. Rev.*, *141*, 5–34.

Auster, H. U., et al. (2008), The THEMIS fluxgate magnetometer, *Space Sci. Rev.*, *141*, 235–264, doi:10.1007/s11214-008-9365-9.

Bell, T. F., U. S. Inan, N. Haque, and J. S. Pickett (2009), Source regions of banded chorus, *Geophys. Res. Lett.*, *36*, L11101, doi:10.1029/2009GL037629.

Bonnell, J. W., F. S. Mozer, G. T. Delory, A. J. Hull, R. E. Ergun, C. M. Cully, V. Angelopoulos, and P. R. Harvey (2008), The Electric Field Instrument (EFI) for THEMIS, *Space Sci. Rev.*, *141*, 303–341, doi:10.1007/s11214-008-9469-2.

Burtis, W. J., and R. A. Helliwell (1969), Banded chorus—A new type of VLF radiation observed in the magnetosphere by OGO 1 and OGO 3, *J. Geophys. Res.*, *74*, 3002–3010, doi:10.1029/JA074i011p03002.

Bianchi, C., and A. Meloni (2007), Natural and man-made terrestrial electromagnetic noise: An outlook, *Ann. Geophys.*, *50*, 435.

Bortnik, J., J. W. Cutler, C. Dunson, and T. E. Bleier (2007), An automatic wave detection algorithm applied to Pc1 pulsations, *J. Geophys. Res.*, *112*, A04204, doi:10.1029/2006JA011900.

Fu, X., et al. (2014), Whistler anisotropy instabilities as the source of banded chorus: Van Allen Probes observations and particle-in-cell simulations, *J. Geophys. Res. Space Physics*, *119*, 8288–8298, doi:10.1002/2014JA020364.

Gao, X. L., W. Li, R. M. Thorne, J. Bortnik, V. Angelopoulos, Q. M. Lu, X. Tao, and S. Wang (2014), New evidence for generation mechanisms of discrete and hiss-like whistler mode waves, *Geophys. Res. Lett.*, *41*, 4905–4811, doi:10.1002/2014GL060707.

LeDocq, M. J., D. A. Guernett, and G. B. Hospodarsky (1998), Chorus source locations from VLF Poynting flux measurements with the Polar spacecraft, *Geophys. Res. Lett.*, *25*(21), 4063, doi:10.1029/1998GL900071.

Li, W., J. Bortnik, R. M. Thorne, and V. Angelopoulos (2011), Global distribution of wave amplitudes and wave normal angles of chorus waves using THEMIS wave observations, *J. Geophys. Res.*, *116*, A12205, doi:10.1029/2011JA017035.

Li, W., R. M. Thorne, J. Bortnik, X. Tao, and V. Angelopoulos (2012), Characteristics of hiss-like and discrete whistler-mode emissions, *Geophys. Rev. Lett.*, *39*, L18106, doi:10.1029/2012GL053206.

Li, W., J. Bortnik, R. M. Thorne, C. M. Cully, L. Chen, V. Angelopoulos, Y. Nishimura, J. B. Tao, J. W. Bonnell, and O. LeContel (2013), Characteristics of the Poynting flux and wave normal vectors of whistler-mode waves observed on THEMIS, *J. Geophys. Res. Space Physics*, *118*, 1461–1471, doi:10.1002/jgra.50176.

Nishimura, Y., et al. (2013), Structures of dayside whistler-mode waves deduced from conjugate diffuse aurora, *J. Geophys. Res. Space Physics*, *118*, 664–673, doi:10.1029/2012JA018242.

Omura, Y., M. Hikishima, Y. Katoh, D. Summers, and S. Yagitani (2009), Nonlinear mechanisms of lower-band and upper-band VLF chorus emissions in the magnetosphere, *J. Geophys. Res.*, *114*, A07217, doi:10.1029/2009JA014206.

Reeves, G. D., et al. (2013), Electron acceleration in the heart of the Van Allen radiation belts, *Science*, *341*, 991–994.

Roux, A., O. Le Contel, C. Coillot, A. Bouabdellah, B. de la Porte, D. Alison, S. Ruocco, and M. C. Vassal (2008), The search coil magnetometer for THEMIS, *Space Sci. Rev.*, *141*(1-4), 265–275, doi:10.1007/s11214-008-9455-8.

Santolik, O., D. A. Gurnett, and J. S. Pickett (2003), Spatio-temporal structure of storm-time chorus, *J. Geophys. Res.*, *108*(A7), 1287, doi:10.1029/2002JA009791.

Smerd, S. F. (1955), Non-linear plasma oscillations and bursts of solar radio emission, *Nature*, *175*, 297, doi:10.1038/175297a0.

Stenflo, L., M. Y. Yu, and P. K. Shukla (1986), Electromagnetic modulations of electron whistlers in plasmas, *J. Plasma Phys.*, *36*, 447.

Tsurutani, B. T., and E. J. Smith (1974), Postmidnight chorus: A substorm phenomenon, *J. Geophys. Res.*, *79*, 118–127, doi:10.1029/JA079i001p00118.

Thorne, R. M., et al. (2013), Rapid local acceleration of relativistic radiation-belt electrons by magnetospheric chorus, *Nature*, *504*, 411–414.

Thorne, R. M., B. Ni, X. Tao, R. B. Horne, and N. P. Meredith (2010), Scattering by chorus waves as the dominant cause of diffuse auroral precipitation, *Nature*, *467*, 943–946.

Verkhoglyadova, O. P., B. T. Tsurutani, and G. S. Lakhina (2010), Properties of obliquely propagating chorus, *J. Geophys. Res.*, *115*, A00F19, doi:10.1029/2009JA014809.

van Milligen, B. P., E. Sanchez, T. Estrada, C. Hidalgo, B. Branas, B. Carreras, and L. Garcia (1995), Wavelet bicoherence: A new turbulence analysis tool, *Phys. Plasmas*, *2*, 3017–3032.

Yoon, P. H., V. S. Pandey, and D.-H. Lee (2014), Oblique nonlinear whistler wave, *J. Geophys. Res. Space Physics*, *119*, 1851–1862, doi:10.1002/2013JA018993.